ACS Sustainable Chemistry & Engineering

pubs.acs.org/journal/ascecg

Research Article

Cooperative External Acidity and Surface Barriers of HZSM-5 in the Coupling Reaction of CH_3Cl and CO to Aromatics

Xudong Fang, Shichao Peng, Mingguan Xie, Zhaopeng Liu, Zhiyang Chen, Hongchao Liu,* Mao Ye, Wenliang Zhu,* and Zhongmin Liu

Cite This: *ACS Sustainable Chem. Eng.* 2023, 11, 2275−2282

Read Online

ACCESS | Metrics & More | Article Recommendations | Supporting Information

ABSTRACT: The acidity and diffusion barriers of zeolites, especially the external surface, are prevailing parameters in the zeolite-catalyzed synthesis of aromatics. Nonetheless, how to well coordinate the external acidity and surface barriers to obtain high benzene−toluene−xylene (BTX) selectivity and exceptional stability remains a great challenge. Herein, we experimentally demonstrate the synergistic effect of external acidity and surface barriers in the coupling of CH_3Cl and CO to aromatics via a surface modification strategy. The results manifest that product selectivity is controlled by external acidity, while catalyst lifetime is controlled by surface barriers. Accordingly, when simultaneously passivating the external acidic sites and reducing the surface barriers, the BTX selectivity was enhanced by 133%, and the catalyst lifetime was prolonged. Our findings provide a new perspective for rational designing of catalysts with superior performance based on controlling the acidity and mass transfer on purpose.

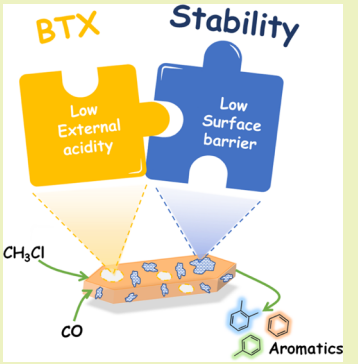

KEYWORDS: *zeolite, external acidity, surface barriers, synergistic effect, CH_3Cl conversion*

INTRODUCTION

Zeolites, as significant microporous materials, have been utilized extensively in acid−base heterogeneous catalysis.[1,2] Due to the adjustable acidity and specific topology, zeolites exhibit unique performance as shape-selective catalysts.[3] Therefore, the key to rational design and efficient utilization of zeolites is based on the comprehensive understanding of the structure−performance relationships. However, the effect of active sites and molecular transport on zeolite catalysis is rather complicated.

Aromatics, notably benzene, toluene, and xylene (BTX), are vital and attractive chemicals, which are mainly produced from petroleum.[4,5] Over the past decade, extensive investigations[6−9] have been conducted to develop novel and sustainable routes for aromatics production via zeolites catalyzing C1 molecules, such as methanol, methane, or derivatives, which can be produced widely from coal, natural gas, and biomass. Recently, we reported an innovative aromatics production strategy from methane enabled by coupling CH_3Cl with CO (CCTA) over H-ZSM-5 owing to its unique acidity and topology.[10] This finding offers a sustainable pathway to alleviate the tremendous stresses on aromatics supply due to the huge reserves of global natural gas. The substantial research studies indicate that ZSM-5 is a superior catalyst for aromatics formation, and its active sites and diffusion play a vital role. Until now, sufficient attempts have been devoted to comprehending the intracrystalline environment of ZSM-5 to improve the aromatics production performance, such as the "confined effect" and intracrystalline diffusion, which established the corresponding reaction−diffusion relationship.[11−14] Thereinto, the intracrystalline diffusion is defined as the guest transport into the intracrystalline environment of zeolites related to the topology of zeolites. Remarkably, recent studies have exhibited that the external surface microenvironment of the ZSM-5 zeolite, that is, the external acidity or surface defects, also dominates a decisive role in the catalytic reaction.[15−18] Consequently, deeply understanding and precisely controlling the external microenvironment of the ZSM-5 zeolite are essential and challenging for rational designing of catalysts with high performance, especially for the CCTA reaction.

Proverbially, the external surface of ZSM-5 is rich in Al, resulting in high external acidity, which is not conducive to shape-selective catalysis.[19] Furthermore, the surface defects on ZSM-5 lead to the change of surface permeability controlling the catalytic reaction rate.[15] Notably, surface permeability is an important mass-transfer parameter related to the penetration of molecules through the surface of zeolites. Thus, significant studies have been dedicated to the crystal surface microenvironment, such as external acidity or surface barriers, through surface modification methods. On the one hand,

Received: September 28, 2022
Revised: December 27, 2022
Published: February 2, 2023

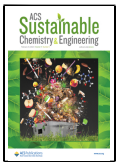

https://doi.org/10.1021/acssuschemeng.2c05822
ACS Sustainable Chem. Eng. 2023, 11, 2275−2282

previous studies, such as chemical liquid/vapor deposition, phosphorus modification, and epitaxial growth, focused on the effect of external acidity without considering the surface barriers resulting from surface passivation and concluded that reducing external acidity can prevent side reactions and external coke deposition.[20−23] On the other hand, modulating surface barriers allows for the regulation of the reactant and product mass transfer through the crystal surface, hence regulating the catalytic efficacy regardless of the changes of external acidity.[24−27] However, it can be concluded easily that even the trivial changes of acidity should be resulted in changing surface barriers and vice versa. Since the complex interrelations between external acidity and surface barriers, independently investigating the effects of surface barriers and external acidity on the production of aromatics over zeolite continues to be an open challenge.

The epitaxial growth of silicate-1 with MFI topology is a typical strategy for the modification of the zeolite surface, controlling the external acidity.[28−32] In doing so, tetraethoxysilane (TEOS) was taken as a precursor for the epitaxial growth of silicate-1 on the external surface of the commercial ZSM-5 zeolite. Due to the large molecular size of TEOS, the intracrystalline properties of the ZSM-5 zeolite can be maintained. Besides, silicate-1 is neutral, and thus, the external acidity over ZSM-5 can be effectively suppressed. Based on the above surface modification strategy, the synergistic effect of surface barriers and external active sites was elucidated by altering the characteristic of the ZSM-5 crystal surface. The structure characterizations revealed that the intracrystalline properties of the modified ZSM-5 hardly change. Nonetheless, the external acidity reduced obviously after modification. In the diffusion evaluation, the surface permeability (α) and the intracrystalline diffusivity (D) have been quantitated carefully, suggesting that the modified ZSM-5 possessed different α but a similar D. The catalytic performance of the parent and modified samples in the CCTA reaction was compared. The BTX selectivity was improved by 133%, and the stability was enhanced over ZSM-5-M1 with the lower external acidity and surface barriers. This work essentially highlighted the fundamental understanding of the synergistic effect of external acidity and surface barriers in zeolite catalysis.

EXPERIMENTAL SECTION

Chemicals and Materials. The ZSM-5 sample was obtained from commercial suppliers. TEOS and tetrapropylammonium hydroxide (TPAOH, 25 wt %, Guangfu Chemical Regent Factory) were used as received without any further purification.

Surface Modification. Commercial HZSM-5 was modified via a TPAOH-directed sol−gel coating process. First, 3.0 g of the HZSM-5 sample was dispersed in a mixture containing TPAOH (1.22 g) and water (30 g) following ultrasonic treatment for 30 min. Then, a different amount of TEOS was added dropwise and stirred for 3 h at 353 K. The mixture was heated in an autoclave at 453 K under static condition for 48 h. After filtration, the samples were washed with distilled water and dried overnight at 383 K. Finally, the samples were calcined at 823 K for 5 h to remove TPAOH. The modified samples are named as ZSM-5-M1, ZSM-5-M2, and ZSM-5-M3, respectively.

Catalyst Characterization. The crystallinity of the samples was characterized by a PANalytical X'Pert PRO powder X-ray diffraction (XRD) meter using a Cu Kα (λ = 0.151 nm) radiation source operated at 40 kV and 40 mA. The composition of zeolites was determined by a Philips Magix-601 X-ray fluorescence (XRF) spectrometer and inductively coupled plasma−atomic emission spectroscopy. The topological images of zeolites were obtained by a Hitachi SU8020 scanning electron microscope operated at 20 kV. The transmission electron microscopy (TEM) images were obtained by a JEM-2100 microscope operating at 200 kV. The nitrogen adsorption−desorption isotherm was measured using a Micromeritics ASAP-2000 apparatus. Before the measurement, the samples were degassed at 523 K to remove the water in zeolites under vacuum for 1 h. The surface area of the samples was estimated by the Brunauer−Emmett−Teller model. The micropore surface area and pore volumes of the samples were calculated by the t-plot method. The pore size distribution was calculated by the density functional theory method. X-ray photoelectron spectroscopy (XPS) spectra were recorded with an ESCALAB 250Xi spectrometer using monochromatized Al Kα radiation. The binding energy of C 1s at 284.8 eV was used as the reference. The uptakes of xylene on the ZSM-5 zeolite were carried out by an intelligent gravimetric analyzer (IGA) equipped with a mesh-type sample cell. The ZSM-5 catalyst (30 mg) was added to the chamber and evacuated at 723 K for 4 h. The increase in mass with the adsorption of xylene over ZSM-5 was measured at 298 K (0−10 mbar).

The acidity of zeolites was measured on a Micromeritics Auto Chem 2920 equipped with a TCD. In brief, 0.15 g of the zeolite sample was loaded into a U-shaped quartz tube and pretreated on 823 K for 30 min in helium. Then, the sample was cooled to 423 K and saturated with NH_3. After removing the physically adsorbed NH_3 in helium, desorption was performed from 423 to 923 K at a heating rate of 10 K/min in He gas. The external acidic properties were obtained from 2,6-di-*tert*-butylpyridine infrared spectra using a Tensor 27 spectrometer with a resolution of 4 cm^{-1}. The samples were pressed into a self-supporting wafer and loaded into an in situ IR cell. Then, the sample was heated to 723 K under vacuum and cooled down to 423 K. The excess of 2,6-di-*tert*-butylpyridine was adsorbed at 423 K, and then the physically adsorbed molecules were removed by evacuation at the same temperature. Fourier transform infrared (FTIR) spectra were recorded on a Broker Tensor 27 spectrometer with a resolution of 4 cm^{-1}. The catalyst was pressed into a self-supporting wafer (radius = 0.65 cm, about 0.014 g) and loaded into an in situ IR cell. Before the measurement, the sample was heated to 673 K for 2 h at vacuum ambiance to remove the physically adsorbed water. After cooling down to room temperature, the spectrum in the region of O−H groups was recorded.

Diffusion Evaluation. The modified dual-resistance model (DRM) was used to fit the uptake curves of xylene measured by IGA, which can obtain α and D following Gao et al.[16] Prior to D, the surface permeability α can be decoupled by means of a quadratic expression derived from Fick's law using the Laplace transform and Taylor's expansion, exhibited as

$$\frac{m_t}{m_\infty}\Big|^{\sqrt{t}\to 0} \cong \frac{\alpha}{l}(\sqrt{t})^2$$

Thereinto, m_t/m_∞, t, and l represent the normalized loading, the uptake time, and the equivalent radius, respectively. The simplified equation can be applied to obtain α by the initial uptake data. After gaining the surface permeability, the intracrystalline diffusivity can be obtained directly through fitting the whole uptake curves with DRM according to

$$\frac{m_t}{m_\infty} = 1 - \sum_{n=1}^{\infty} \frac{2L^2 \exp\left(-\frac{\beta_n^2 Dt}{l^2}\right)}{(\beta_n^2 + L^2 + L)\beta_n^2}; \qquad \beta_n \tan \beta_n = L = \frac{\alpha l}{D}$$

Based on the above methods, the information of surface barriers and intracrystalline diffusivity can be quantificationally gained by fitting the uptake curves of xylene.

Catalyst Evaluation. ZSM-5 and modified ZSM-5 were evaluated in our work. In brief, 0.15 g of the prepared sample was loaded in a high-pressure fixed-bed flow reactor (inside diameter = 7 mm) made by stainless steel. The catalyst bed was held between two quartz wool plugs. Prior to the reaction, the catalyst was first heated in flowing nitrogen (flow rate, 40 mL/min) at 723 K for 3 h to remove water in the zeolite and then cooled down to the reaction temperature.

https://doi.org/10.1021/acssuschemeng.2c05822
ACS Sustainable Chem. Eng. 2023, 11, 2275−2282

Subsequently, a certain amount of CH_3Cl and CO was introduced into the reactor at a fixed pressure.

All the effluent products were analyzed by online gas chromatographs (Agilent 7890A) equipped with a PLOT-Q capillary column which was connected to a flame ionization detector. The CH_3Cl conversion and product selectivity were calculated on a molar carbon basis.

$$\text{Conv } CH_3Cl = \frac{\sum_1^n nC_nH_mO_{l_{outlet}} - CH_3Cl_{outlet}}{\sum_1^n nC_nH_mO_{l_{outlet}}} \times 100\%$$

$$\text{sel product } X = \frac{\text{products } X_{outlet}}{\sum_1^n nC_nH_mO_{l_{outlet}} - CH_3Cl_{outlet}} \times 100\%$$

Thereinto, $nC_nH_mO_{l_{outlet}}$, CH_3Cl_{outlet}, and product X_{outlet} represent the carbon atoms of $nC_nH_mO_{l_{outlet}}$ at the outlet, carbon atoms of CH_3Cl_{outlet} at the outlet, and carbon atoms of product X_{outlet} at the outlet, respectively.

RESULTS AND DISCUSSION

Fabrication and Structural Characterization. For directional regulation of the surface microenvironment of ZSM-5, the epitaxial growth of silicate-1 was adopted as a modification strategy. The pristine samples were denoted as ZSM-5-P, and the in situ growth of silicate-1 was controlled to obtain coupled ZSM-5 samples with different surface barriers and external acidity, denoted as ZSM-5-M1, ZSM-5-M2, and ZSM-5-M3, respectively (Scheme 1).

Scheme 1. Schematic Diagram of the Fabrication-Modified ZSM-5

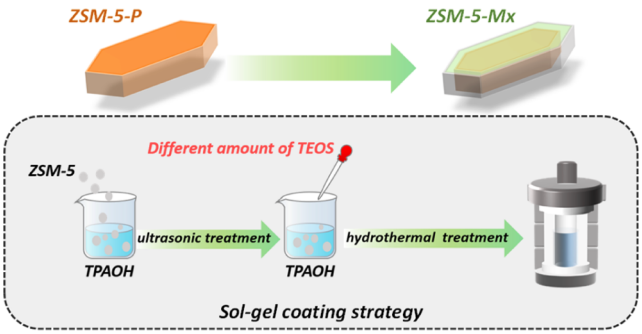

The variations of the structure of modified ZSM-5 were thoroughly investigated. All the samples preserved typical coffin-shaped crystals with uniform particle sizes (~3 μm), as shown by scanning electron microscopy (SEM) images (Figure 1a–d). Notably, the surface roughness changed, and many protrusions are observed on ZSM-5-M2 and ZSM-5-M3. Furthermore, Figure 1 also exhibits the distribution of Al over the surface of the four samples. The signal of Al is obviously weakened after surface modification. Figure S1 in the Supporting Information exhibited the TEM images of ZSM-5 and modified ZSM-5. By increasing the amount of TEOS, the thickness of the shell increased from 0 to 133 nm. These results suggested that the silicon species successfully coated the surface of ZSM-5. Additionally, the contact angle has been measured, as shown in Figure 1e–h. The contact angle of ZSM-5-P is almost 0°, whereas the modified ZSM-5 shows certain hydrophobicity. In particular, ZSM-5-M1 exhibited the largest contact angle (16.7°). Therefore, we can conclude that the surface of ZSM-5 has been covered with TEOS, leading to the change of surface element distribution and roughness.

Ulteriorly, the Si/Al molar ratio (Table S1 in the Supporting Information), as determined by XRF, steadily increased with increasing TEOS addition. Additionally, Figure 2a depicts the Al 2p scan of the surface of each sample. After modification, the peak intensity obviously dropped. The surface Si/Al, determined by XPS, also increased from 21.2 to 104.8 with increasing TEOS addition (Table S1 in the Supporting Information). These results validated that silicate-1 effectively covered the external surface of ZSM-5. Moreover, the XRD patterns of the four samples (Figure 2b) showed five characteristic peaks of the MFI structure at 7.9°, 8.9°, 23.1°, 23.3°, and 23.9°, suggesting that epitaxial growing silicate-1 did not change the original crystal structure. Based on these results, we also synthesized silicate-1 under the same conditions without ZSM-5, which exhibited the typical MFI peaks (Figure S2 in the Supporting Information) and coffin-shaped samples (Figure S3 in the Supporting Information). These results revealed that the surface modification cannot affect the structure of ZSM-5 theoretically. As can be seen in Figure 2c, typical type I isotherms were observed, revealing that all of the samples were microporous zeolites. Table S2 in the Supporting Information also shows that all the samples had a similar surface area and pore volume. Moreover, a slight change in micropore volume (from 0.10 to 0.07) was observed, indicating that the modification strategy inevitably resulted in the formation of a small number of mesopores. Additionally, Figure 2d also shows that all the samples had a similar micropore size distribution (~0.68 nm), suggesting that the micropore size is hardly affected. Remarkably, as shown in Figure S4 in the Supporting Information, the similar mesopore size distribution (~2 nm) of all the samples demonstrated that the modification had little effect on the internal structure of zeolites and would not lead to the formation of larger mesopores. Therefore, it can be summarized that all of the four samples had the same intracrystalline properties after modification.

Acidic Properties. The acidic properties of ZSM-5 after modification were carefully measured. According to the NH_3-TPD curves (Figure 3a), two peaks appeared at 509 and 700 K, respectively, corresponding to the weak and strong acidic sites. By increasing the addition of TEOS, the total amount of acidic sites decreased from 0.51 to 0.29 mmol/g (Table S3 in the Supporting Information). Note that the peak of the weak acidic sites shifted toward the low temperature when the addition of TEOS increased. As shown in Table S3 in the Supporting Information, the amount of weak acidity and strong acidity also decreased with increasing TEOS addition. The change in acidity indicated that silicate-1 covers the external acidic sites. Furthermore, 2,6-di-*tert*-butylpyridine IR spectroscopy was employed to evaluate the external acidity. The signal at 1614 cm^{-1} in Figure 3b corresponded to the interaction of the probe molecule with the exterior surface acidic sites.[33] Table S3 in the Supporting Information exhibits that with increasing amount of TEOS, the amount of external acidity decreased from 14.9 to 4.1 μmol/g. These results were consistent with the result of XPS, demonstrating that the external acidity decreased gradually. Thus, the external acidity for the four ZSM-5 samples is as follows: ZSM-5-P > ZSM-5-M1 > ZSM-5-M2 > ZSM-5-M3. The FTIR spectroscopy results of the four ZSM-5 samples are shown in Figure S5 in the Supporting Information. After modifications, the peak at 3610 cm^{-1} assigned to bridging hydroxyl groups decreased, which might be attributed to the reduction of acidity. Combined with the

https://doi.org/10.1021/acssuschemeng.2c05822
ACS Sustainable Chem. Eng. 2023, 11, 2275−2282

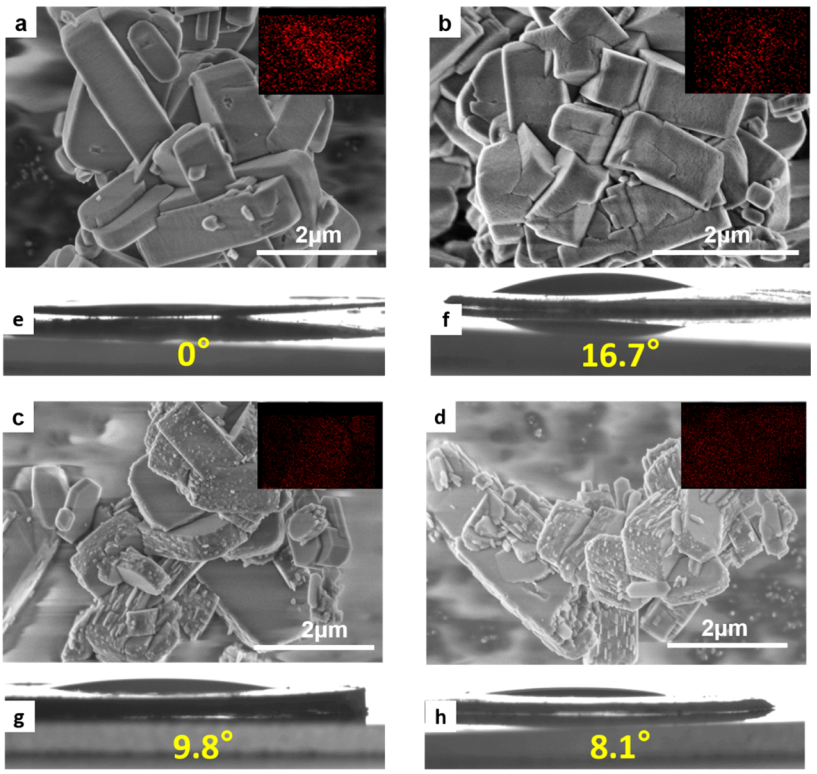

Figure 1. (a–d) SEM images and the corresponding EDX mapping representing Al and (e–h) contact angle of the four ZSM-5 samples.

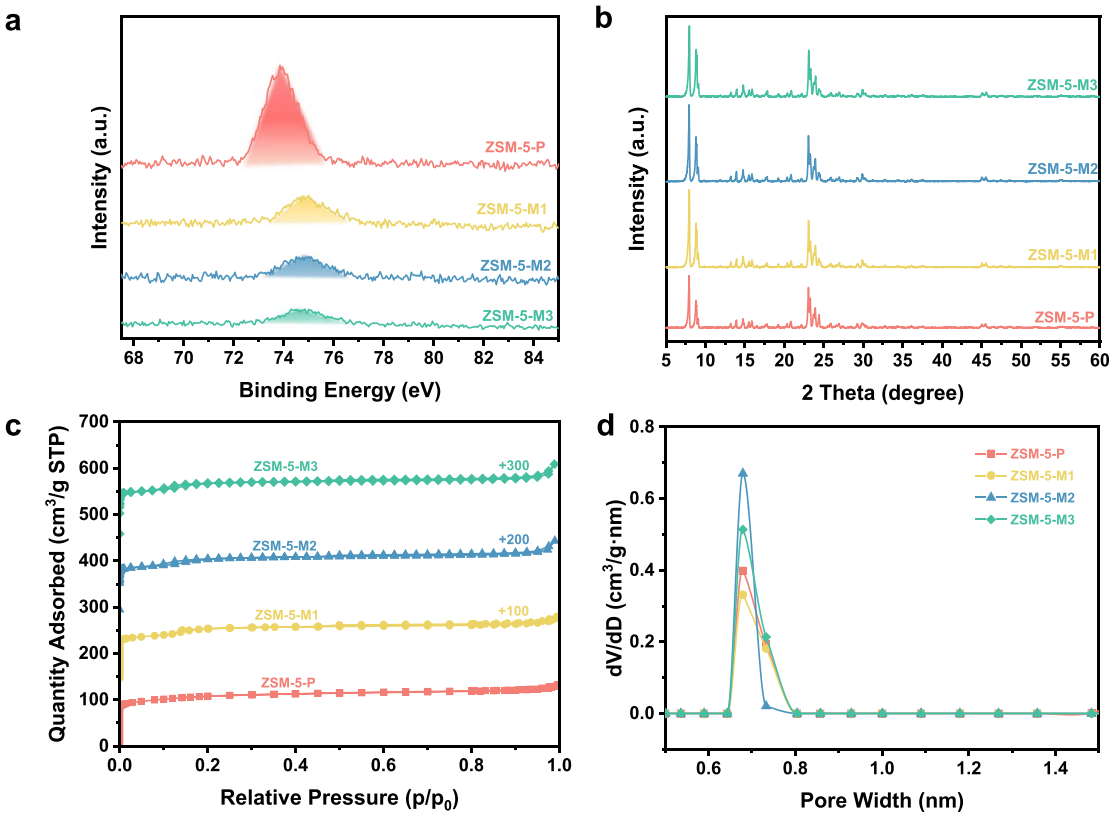

Figure 2. (a) Al 2p XPS spectra, (b) XRD patterns, (c) N_2 adsorption–desorption isotherms, and (d) micropore size distribution of the four ZSM-5 samples.

above results, we speculated that the reduction of peak intensity at 3610 cm^{-1} might be caused by the weakening of the external acidity. Interestingly, the broad peak at around 3420 cm^{-1} attributing to silanol nests almost disappeared over ZSM-5-M1 and returned over ZSM-5-M2 and ZSM-5-M3. Typically, silanol nests are formed at crystal steps or extended

https://doi.org/10.1021/acssuschemeng.2c05822
ACS Sustainable Chem. Eng. 2023, 11, 2275–2282

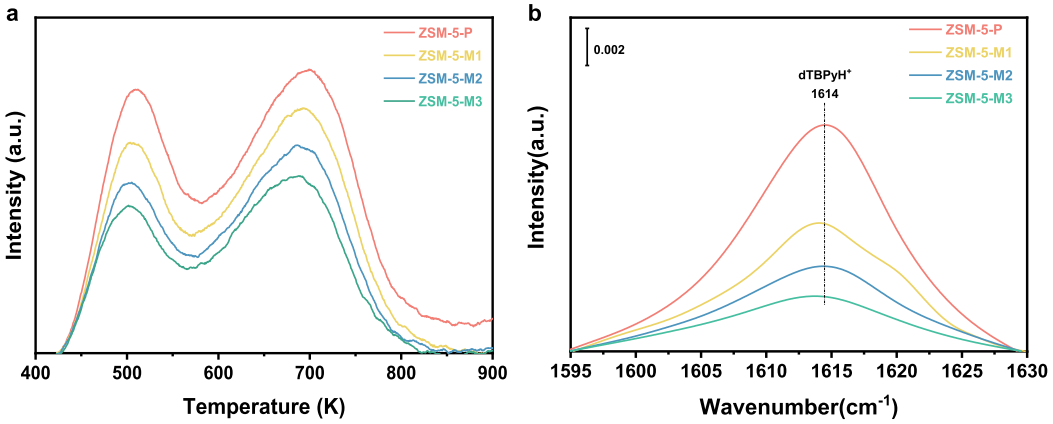

Figure 3. (a) NH_3-TPD files and (b) IR spectra of 2,6-di-*tert*-butylpyridine of the four ZSM-5 samples.

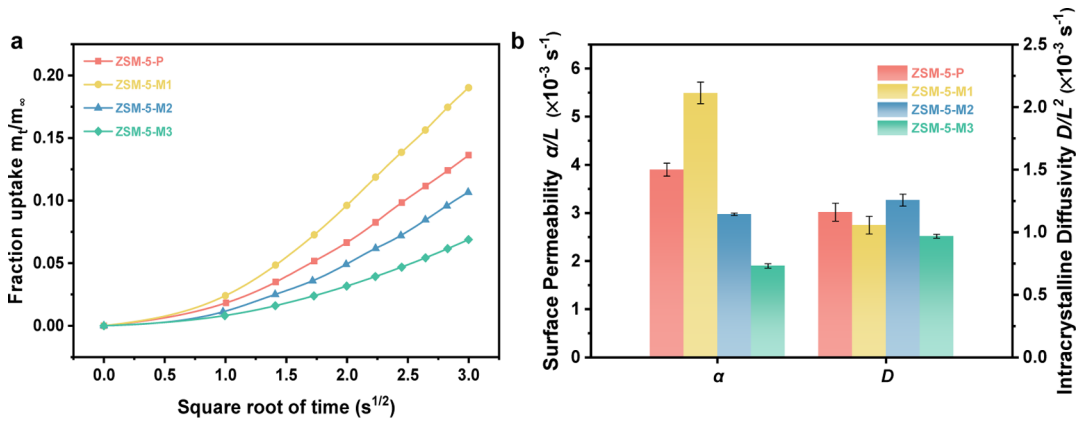

Figure 4. (a) Initial uptake rate of xylene at 298 K and (b) surface permeability and intracrystalline diffusivity of xylene based on the uptake rates (Figure S6 in the Supporting Information) calculated via the method of Gao et al.[16]

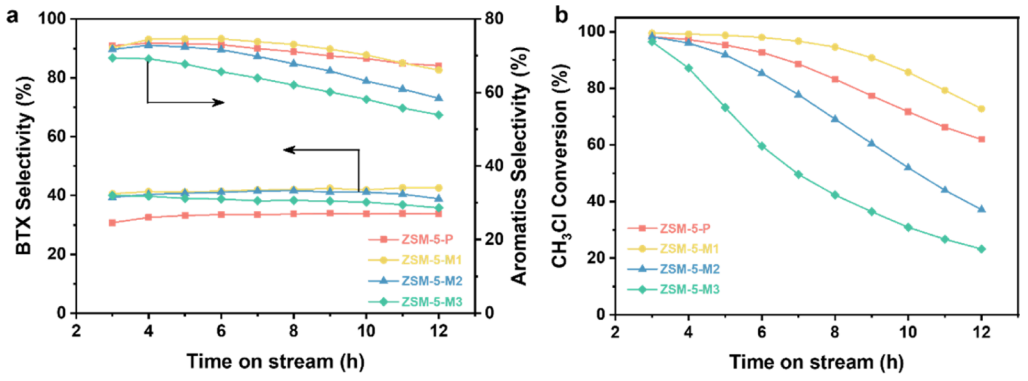

Figure 5. (a) BTX selectivity and aromatics selectivity (b) CH_3Cl conversion as a function of time on stream in CCTA reaction over the four ZSM-5 samples. Reaction conditions: 673 K, P_{CO} = 1.72 MPa, P_{CH3Cl} = 0.014 MPa, 9600 mL/g_{cat}/h, and Ar as balance gas.

defects which might lead to the formation of mass-transfer limitations.[34,35] This observation implied that the surface barriers might be modulated by epitaxial growing silicate-1. Thus, the textural and acidic results above showed that ZSM-5 and modified ZSM-5 exhibited similar intracrystalline properties but vary in external acidity.

Quantitative Diffusion Properties. The diffusion characteristics of the four ZSM-5 samples were obtained using an IGA. These parameters included surface permeability (α) and intracrystalline diffusivity (D). In the uptake rate measurement, xylene, accounting for the largest proportion of aromatics in CCTA reaction, was chosen as a guest molecule. The uptake curves of xylene at 298 K are presented in Figures 4a and S6 in the Supporting Information, which were applied to calculate the α and D values using Gao et al.'s approach.[16] As can be seen in Figure 4b, the four ZSM-5 samples had comparable D values, which was related to the similar intracrystalline characteristics after alteration. Nevertheless, different α values were seen for all the samples, which followed as the order of ZSM-5-M1, ZSM-5, ZSM-5-M2, and ZSM-5-M3. The difference was in accordance with our above characterizations of structural morphology. Consequently, these results indicated that the epitaxial growth of silicate-1 can modulate the surface barriers and maintain the property of intracrystalline diffusion.

https://doi.org/10.1021/acssuschemeng.2c05822
ACS Sustainable Chem. Eng. 2023, 11, 2275−2282

Catalytic Performance in the CCTA Reaction. The CCTA reaction was performed using the four ZSM-5 samples under reaction conditions of 673 K, 2.0 MPa, and 9600 mL/g_{cat}/h. Figure 5 illustrates the aromatics selectivity, BTX selectivity, and CH_3Cl conversion, respectively, as a function of time. The initial aromatics selectivity over all the ZSM-5 samples changed slightly maintaining at about 70%. However, the BTX selectivity over the modified ZSM-5 increased by ca. 133%. The improvement in BTX selectivity demonstrated that the secondary reaction of products was inhibited due to the surface modification of ZSM-5, which was consistent with the previous studies.[32] Furthermore, the catalyst stability of the modified samples was studied, as shown in Figure 5b. Not all the modified samples have improved the catalyst stability, following ZSM-5-M1 > ZSM-5-P > ZSM-5-M2 > ZSM-5-M3, which was inconsistent with the previous studies on the external acidity.[36] Thus, considering similar intracrystalline properties for the four ZSM-5 samples, the change in catalytic performance should be related to the external surface microenvironment, including external acidity and surface barriers.

The relationship of catalytic performance and external microenvironment was further discussed. Compared with ZSM-5-P, ZSM-5-M2 and ZSM-5-M3 significantly decreased the external acidity and surface permeability, exhibiting increased BTX selectivity but decreased stability. Therefore, we concluded that reducing the external acidity can improve the BTX selectivity. Additionally, the shortening of catalyst lifetime might be mainly related to the surface barriers due to the same intracrystalline properties. To further confirm the role of surface barriers, the catalytic performance of ZSM-5-M1, ZSM-5-M2, and ZSM-5-M3 was explored. Although the BTX selectivity of the three samples all increased due to the reduction of external acidity, the catalyst lifetime is shortened with increasing surface barriers. This result confirmed that reducing the surface barriers can effectively enhance the catalyst stability. Ulteriorly, ZSM-5-M1 revealed the decreased surface barriers and external acidity, compared with ZSM-5-P, which drop the probability of secondary reaction, such as alkylation, dealkylation, isomerization, and hydrogen transfer reactions, to enhance the diffusion of reactants and products. The BTX selectivity and catalyst lifetime can be improved correspondingly (Figure 5). These results further verified the correctness of the conclusion that the external acidity could control the product selectivity, and the surface barriers could affect the stability of the catalyst. Thus, coordinating the relationship of external acidity and surface barriers can obtain the perfect catalytic performance.

CONCLUSIONS

In summary, we experimentally confirmed the synergistic effect of external acidity and surface barriers of the ZSM-5 zeolite in the CCTA reaction via a surface modification strategy. Combined with the structure, acid property characterization, and catalytic performance, the role of external acidity and surface barriers were recognized, whose product selectivity was controlled by the former and the catalyst lifetime was dominated by the latter. When reducing the external acidity while maintaining lower surface barriers, based on our understanding, the BTX selectivity was enhanced by 133% and the catalyst lifetime was prolonged. This work provides a strategy for the enhancement of reaction performance in zeolite catalysis via coordinating the external acidity and surface barriers.

ASSOCIATED CONTENT

Supporting Information

The Supporting Information is available free of charge at https://pubs.acs.org/doi/10.1021/acssuschemeng.2c05822.

TEM images, XRD patterns, SEM images, mesopore size distribution, DRIFT spectra, IGA curves, Si/Al ratio, textural properties, and Bronsted acidity (PDF)

AUTHOR INFORMATION

Corresponding Authors

Hongchao Liu − *National Engineering Research Center of Lower-Carbon Catalysis Technology, Dalian Institute of Chemical Physics, Chinese Academy of Sciences, 116023 Dalian, China*; Email: chliu@dicp.ac.cn

Wenliang Zhu − *National Engineering Research Center of Lower-Carbon Catalysis Technology, Dalian Institute of Chemical Physics, Chinese Academy of Sciences, 116023 Dalian, China*; orcid.org/0000-0002-2247-6849; Email: wlzhu@dicp.ac.cn

Authors

Xudong Fang − *National Engineering Research Center of Lower-Carbon Catalysis Technology, Dalian Institute of Chemical Physics, Chinese Academy of Sciences, 116023 Dalian, China; University of Chinese Academy of Sciences, 100049 Beijing, China*

Shichao Peng − *National Engineering Research Center of Lower-Carbon Catalysis Technology, Dalian Institute of Chemical Physics, Chinese Academy of Sciences, 116023 Dalian, China; University of Chinese Academy of Sciences, 100049 Beijing, China*

Mingguan Xie − *National Engineering Research Center of Lower-Carbon Catalysis Technology, Dalian Institute of Chemical Physics, Chinese Academy of Sciences, 116023 Dalian, China; University of Chinese Academy of Sciences, 100049 Beijing, China*

Zhaopeng Liu − *National Engineering Research Center of Lower-Carbon Catalysis Technology, Dalian Institute of Chemical Physics, Chinese Academy of Sciences, 116023 Dalian, China; University of Chinese Academy of Sciences, 100049 Beijing, China*

Zhiyang Chen − *National Engineering Research Center of Lower-Carbon Catalysis Technology, Dalian Institute of Chemical Physics, Chinese Academy of Sciences, 116023 Dalian, China; University of Chinese Academy of Sciences, 100049 Beijing, China*

Mao Ye − *National Engineering Research Center of Lower-Carbon Catalysis Technology, Dalian Institute of Chemical Physics, Chinese Academy of Sciences, 116023 Dalian, China*; orcid.org/0000-0002-7078-2402

Zhongmin Liu − *National Engineering Research Center of Lower-Carbon Catalysis Technology, Dalian Institute of Chemical Physics, Chinese Academy of Sciences, 116023 Dalian, China; University of Chinese Academy of Sciences, 100049 Beijing, China*; orcid.org/0000-0002-7999-2940

Complete contact information is available at: https://pubs.acs.org/10.1021/acssuschemeng.2c05822

Author Contributions

X.D.F. and S.C.P. contributed equally. Z.M.L., W.L.Z., H.C.L, M.Y., X.D.F., and S.C.P. contributed to conceptualization; X.D.F., S.C.P, H.C.L., M.G.X., Z.P.L., and Z.Y.C. contributed to investigation; X.D.F. and S.C.P. contributed to validation; X.D.F. and S.C.P. contributed to writing—original draft; X.D.F. and H.C.L. contributed to visualization; W.L.Z., M.Y., and H.C.L. contributed to writing—review and editing; and W.L.Z. and H.C.L contributed to supervision.

Notes

The authors declare no competing financial interest.

All data needed to evaluate the conclusions in the paper are present in the paper and/or the Supporting Information. Additional data related to this paper may be requested from the authors.

■ ACKNOWLEDGMENTS

This work was supported by the National Natural Science Foundation of China (grant nos. 21972141, 21991094, and 21991090) and the "Transformational Technologies for Clean Energy and Demonstration", Strategic Priority Research Program of the Chinese Academy of Sciences (grant no. XDA21030100), the Dalian High Level Talent Innovation Support Program (2017RD07), and the National Special Support Program for High Level Talents (SQ2019RA2TST0016). The authors thank Peifang Yan and Wenguang Yu in the Dalian Institute of Chemical Physics, Chinese Academy of Sciences, for the help with IGA measurement.

■ REFERENCES

(1) Zhang, Q.; Yu, J.; Corma, A. Applications of Zeolites to C1 Chemistry: Recent Advances, Challenges, and Opportunities. *Adv. Mater.* **2020**, *32*, 2002927.

(2) Li, Y.; Yu, J. Emerging applications of zeolites in catalysis, separation and host−guest assembly. *Nat. Rev. Mater.* **2021**, *6*, 1156−1174.

(3) Chen, L. H.; Sun, M. H.; Wang, Z.; Yang, W.; Xie, Z.; Su, B. L. Hierarchically Structured Zeolites: From Design to Application. *Chem. Rev.* **2020**, *120*, 11194−11294.

(4) Spivey, J. J.; Hutchings, G. Catalytic aromatization of methane. *Chem. Soc. Rev.* **2014**, *43*, 792−803.

(5) Li, T.; Shoinkhorova, T.; Gascon, J.; Ruiz-Martínez, J. Aromatics Production via Methanol-Mediated Transformation Routes. *ACS Catal.* **2021**, *11*, 7780−7819.

(6) Chen, Z.; Ni, Y.; Zhi, Y.; Wen, F.; Zhou, Z.; Wei, Y.; Zhu, W.; Liu, Z. Coupling of Methanol and Carbon Monoxide over H-ZSM-5 to Form Aromatics. *Angew. Chem., Int. Ed. Engl.* **2018**, *57*, 12549−12553.

(7) Wen, F.; Zhang, J.; Chen, Z.; Zhou, Z.; Liu, H.; Zhu, W.; Liu, Z. Coupling conversion of methane with carbon monoxide via carbonylation over Zn/HZSM-5 catalysts. *Catal. Sci. Technol.* **2021**, *11*, 1358−1364.

(8) Shoinkhorova, T.; Cordero-Lanzac, T.; Ramirez, A.; Chung, S.-h.; Dokania, A.; Ruiz-Martinez, J.; Gascon, J. Highly Selective and Stable Production of Aromatics via High-Pressure Methanol Conversion. *ACS Catal.* **2021**, *11*, 3602−3613.

(9) Chen, H.; Chen, T.; Chen, K.; Fu, J.; Lu, X.; Ouyang, P. Catalytic aromatization of methyl bromide to aromatics over bimetallic CuO-ZnO/HZSM-5. *Catal. Commun.* **2018**, *103*, 38−41.

(10) Fang, X.; Liu, H.; Chen, Z.; Liu, Z.; Ding, X.; Ni, Y.; Zhu, W.; Liu, Z. Highly Enhanced Aromatics Selectivity by Coupling of Chloromethane and Carbon Monoxide over H-ZSM-5. *Angew. Chem., Int. Ed. Engl.* **2022**, *61*, No. e202114953.

(11) Liu, X.; Shi, J.; Yang, G.; Zhou, J.; Wang, C.; Teng, J.; Wang, Y.; Xie, Z. A diffusion anisotropy descriptor links morphology effects of H-ZSM-5 zeolites to their catalytic cracking performance. *Commun. Chem.* **2021**, *4*, 107.

(12) Grifoni, E.; Piccini, G.; Lercher, J. A.; Glezakou, V. A.; Rousseau, R.; Parrinello, M. Confinement effects and acid strength in zeolites. *Nat. Commun.* **2021**, *12*, 2630.

(13) Guo, Z.; Li, X.; Hu, S.; Ye, G.; Zhou, X.; Coppens, M.-O. Understanding the Role of Internal Diffusion Barriers in Pt/Beta Zeolite Catalyzed Isomerization of n-Heptane. *Angew. Chem., Int. Ed. Engl.* **2020**, *59*, 1548−1551.

(14) Lin, L.; Fan, M.; Sheveleva, A. M.; Han, X.; Tang, Z.; Carter, J. H.; da Silva, I.; Parlett, C. M. A.; Tuna, F.; McInnes, E. J. L.; et al. Control of zeolite microenvironment for propene synthesis from methanol. *Nat. Commun.* **2021**, *12*, 822.

(15) Rao, S. M.; Saraçi, E.; Gläser, R.; Coppens, M.-O. Surface barriers as dominant mechanism to transport limitations in hierarchically structured catalysts − Application to the zeolite-catalyzed alkylation of benzene with ethylene. *Chem. Eng. J.* **2017**, *329*, 45−55.

(16) Gao, M.; Li, H.; Yang, M.; Gao, S.; Wu, P.; Tian, P.; Xu, S.; Ye, M.; Liu, Z. Direct quantification of surface barriers for mass transfer in nanoporous crystalline materials. *Commun. Chem.* **2019**, *2*, 43.

(17) Guefrachi, Y.; Sharma, G.; Xu, D.; Kumar, G.; Vinter, K. P.; Abdelrahman, O. A.; Li, X.; Alhassan, S.; Dauenhauer, P. J.; Navrotsky, A.; et al. Steam-Induced Coarsening of Single-Unit-Cell MFI Zeolite Nanosheets and Its Effect on External Surface Bronsted Acid Catalysis. *Angew. Chem., Int. Ed. Engl.* **2020**, *59*, 9579−9585.

(18) Almutairi, S. M. T.; Mezari, B.; Filonenko, G. A.; Magusin, P. C. M. M.; Rigutto, M. S.; Pidko, E. A.; Hensen, E. J. M. Influence of Extraframework Aluminum on the Brønsted Acidity and Catalytic Reactivity of Faujasite Zeolite. *ChemCatChem* **2013**, *5*, 452−466.

(19) Kim, K.; Ryoo, R.; Jang, H.-D.; Choi, M. Spatial distribution, strength, and dealumination behavior of acid sites in nanocrystalline MFI zeolites and their catalytic consequences. *J. Catal.* **2012**, *288*, 115−123.

(20) Giordano, G.; Migliori, M.; Ferrarelli, G.; Giorgianni, G.; Dalena, F.; Peng, P.; Debost, M.; Boullay, P.; Liu, Z.; Guo, H.; et al. Passivated Surface of High Aluminum Containing ZSM-5 by Silicalite-1: Synthesis and Application in Dehydration Reaction. *ACS Sustainable Chem. Eng.* **2022**, *10*, 4839−4848.

(21) Zhang, J.; Qian, W.; Kong, C.; Wei, F. Increasing para-Xylene Selectivity in Making Aromatics from Methanol with a Surface-Modified Zn/P/ZSM-5 Catalyst. *ACS Catal.* **2015**, *5*, 2982−2988.

(22) Xu, G.; Zhu, X. A core-shell structured Zn/SiO_2@ZSM-5 catalyst: Preparation and enhanced catalytic properties in methane co-aromatization with propane. *Appl. Catal., B* **2021**, *293*, 120241.

(23) Lv, J.; Hua, Z.; Zhou, J.; Liu, Z.; Guo, H.; Shi, J. Surface-Passivated Hierarchically Structured ZSM-5 Zeolites: High-Performance Shape-Selective Catalysts for para-Xylene Production. *ChemCatChem* **2018**, *10*, 2278−2284.

(24) Peng, S.; Gao, M.; Li, H.; Yang, M.; Ye, M.; Liu, Z. Control of Surface Barriers in Mass Transfer to Modulate Methanol-to-Olefins Reaction over SAPO-34 Zeolites. *Angew. Chem., Int. Ed. Engl.* **2020**, *59*, 21945−21948.

(25) Peng, S.; Xie, Y.; Wang, L.; Liu, W.; Li, H.; Xu, Z.; Ye, M.; Liu, Z. Exploring the Influence of Inter- and Intra-crystal Diversity of Surface Barriers in Zeolites on Mass Transport by Using Super-Resolution Microimaging of Time-Resolved Guest Profiles. *Angew. Chem., Int. Ed. Engl.* **2022**, *61*, No. e202203903.

(26) Peng, S.; Li, H.; Liu, W.; Yu, J.; Xu, Z.; Ye, M.; Liu, Z. Reaction rate enhancement by reducing surface diffusion barriers of guest molecules over ZSM-5 zeolites: a structured illumination microscopy study. *Chem. Eng. J.* **2022**, *430*, 132760.

(27) Hu, S.; Liu, J.; Ye, G.; Zhou, X.; Coppens, M. O.; Yuan, W. Effect of External Surface Diffusion Barriers on Platinum/Beta-Catalyzed Isomerization of n-Pentane. *Angew. Chem., Int. Ed. Engl.* **2021**, *60*, 14394−14398.

(28) Vanvu, D.; Miyamoto, M.; Nishiyama, N.; Egashira, Y.; Ueyama, K. Selective formation of para-xylene over H-ZSM-5 coated with polycrystalline silicalite crystals. *J. Catal.* **2006**, *243*, 389−394.

https://doi.org/10.1021/acssuschemeng.2c05822
ACS Sustainable Chem. Eng. 2023, 11, 2275−2282

(29) Van Vu, D.; Miyamoto, M.; Nishiyama, N.; Egashira, Y.; Ueyama, K. Morphology Control of Silicalite/HZSM-5 Composite Catalysts for the Formation of Para-Xylene. *Catal. Lett.* **2008**, *127*, 233−238.
(30) Vu, D. V.; Miyamoto, M.; Nishiyama, N.; Ichikawa, S.; Egashira, Y.; Ueyama, K. Catalytic activities and structures of silicalite-1/H-ZSM-5 zeolite composites. *Microporous Mesoporous Mater.* **2008**, *115*, 106−112.
(31) Miyamoto, M.; Kamei, T.; Nishiyama, N.; Egashira, Y.; Ueyama, K. Single Crystals of ZSM-5/Silicalite Composites. *Adv. Mater.* **2005**, *17*, 1985−1988.
(32) Miyamoto, M.; Ono, S.; Oumi, Y.; Uemiya, S.; Van der Perre, S.; Virdis, T.; Baron, G. V.; Denayer, J. F. M. Nanoporous ZSM-5 Crystals Coated with Silicalite-1 for Enhanced p-Xylene Separation. *ACS Appl. Nano Mater.* **2019**, *2*, 2642−2650.
(33) Góra-Marek, K.; Tarach, K.; Choi, M. 2,6-Di-tert-butylpyridine Sorption Approach to Quantify the External Acidity in Hierarchical Zeolites. *J. Phys. Chem. C* **2014**, *118*, 12266−12274.
(34) Zhang, J.; Zhu, X.; Wang, G.; Wang, P.; Meng, Z.; Li, C. The origin of the activity and selectivity of silicalite-1 zeolite for toluene methylation to para -xylene. *Chem. Eng. J.* **2017**, *327*, 278−285.
(35) Bordiga, S.; Roggero, I.; Ugliengo, P.; Zecchina, A.; Bolis, V.; Artioli, G.; Buzzoni, R.; Marra, G.; Rivetti, F.; Spanò, G.; et al. Characterisation of defective silicalites. *J. Chem. Soc., Dalton Trans.* **2000**, *21*, 3921−3929.
(36) Goodarzi, F.; Herrero, I. P.; Kalantzopoulos, G. N.; Svelle, S.; Lazzarini, A.; Beato, P.; Olsbye, U.; Kegnæs, S. Synthesis of mesoporous ZSM-5 zeolite encapsulated in an ultrathin protective shell of silicalite-1 for MTH conversion. *Microporous Mesoporous Mater.* **2020**, *292*, 109730.

https://doi.org/10.1021/acssuschemeng.2c05822
ACS Sustainable Chem. Eng. 2023, 11, 2275−2282